Macromolecular Research, Vol. 14, No. 6, pp 603-609 (2006)

Macroscopic Nonlinear Optical Properties of Tricyanopyrrolidene Chromophore Containing Amorphous Polycarbonate: Effect of Molecular Lateral Moiety in the Conjugative Structure

Min Ju Cho, Sang Kyu Lee, Jung-Il Jin, and Dong Hoon Choi*

Department of Chemistry, Center for Electro- & Photo-Responsive Molecules, Korea University, Seoul 136-701, Korea

Received July 18, 2006; Revised October 12, 2006

Abstract: Tricyanopyrrolidene chromophores were prepared in order to compare their macroscopic nonlinear optical (NLO) properties with a conjugated structure through the long molecular axis. A thiophene or phenyl ring was tethered to an ethylenic bond; it may act as a lateral moiety to disrupt the planarity of a chromophore and lessen the electrostatic interaction. Thin film composites of these chromophores dissolved in amorphous polycarbonate (APC) were fabricated. Real time pole and probe method was employed to investigate the change of electro-optic (EO) signal during poling. The EO properties and their relaxation behaviors of the guest-host systems containing newly synthesized chromophores were investigated in detail.

Keywords: tricyanopyrrolidene chromophore, electro-optic effect, *in-situ* pole and probe, organic photonic material.

Introduction

Organic chromophores having large molecular hyperpolarizabilitiy (β) values, as well as the polymeric composites containing them have drawn much attention over the past two decades.[1-5] Factors such as high NLO susceptibility, fast response time, low dielectric constant, small dispersion in the refractive index, structural flexibility, and ease of material processing are advantageous in organic NLO materials systems.[6-10] To achieve good device functionality, NLO chromophores have to possess the following criterion simultaneously: high microscopic molecular nonlinearity ($\mu\beta(0)$), good thermal stability and photostability, low absorption, and weak molecular electrostatic interaction in the polymer matrix.[11,12]

Much effort was made to develop the NLO chromophore with a high molecular hyperpolarizability, β and to improve thermal/photo-stability.[13,14] Recently, very large nonlinearities were achieved by employing a heterocyclic ring molecular unit such as thiophene or thiazole since they have lower resonance stabilization energies upon charge delocalization than benzene rings.[15-17] Some electron-deficient heterocyclic molecules have been known as strong acceptors for NLO materials.[18] Particularly, 2-cyanomethylene-3-cyano-4,5,5-trimethyl-2,5-dihydrofuran (TCF) is frequently employed as a strong electron acceptor that induces significantly high dipole moment (μ), first-order molecular hyperpolarizability (β), and their product ($\mu\beta$). The NLO chromophores bearing TCF have been used for electro-optic (EO) device and photorefractive applications.[19-21]

In order to achieve high macroscopic optical nonlinearity, electric field poling or unique molecular assembly techniques are used to be employed to achieve a bulk acentric ordering of the molecular lattice. In this study, a thiophene or phenyl unit in an ethylenic bond was used as a lateral moiety to disrupt planar geometry for lessening intermolecular interaction.

As intermolecular electrostatic force becomes higher than poling force, we observe the decreasing behavior of the EO signal over a certain chromophore density at cooling process even in the presence of the poling electric field. Additionally, when the dipole moment of the chromophore is quite high enough to order in an antiparallel way, the molecules are easily interacted each other. Although the microscopic nonlinearity ($\mu\beta(0)$) of the planar and highly polar chromophore is relatively high, the macroscopic nonlinearity in the polymer matrix induced by electric field poling process may not exhibit correspondingly. Recently, Jen *et al.* firstly reported the strong potential of pyrroline chromophore and their detailed microscopic analysis data.[22]

In this report, we described the EO properties of amorphous polycarbonate (APC) samples bearing new chromophores. We selected 2-(1-allyl-3-cyano-4-methyl-5-oxo-1,5-dihydropyrrol-2-ylidene)-malononitrile (TCP) as an acceptor to synthesize new chromophores. Electrochemical method and absorption spectroscopy were employed to study their molecular energy levels for estimating microscopic nonlin-

*Corresponding Author. E-mail: dhchoi8803@korea.ac.kr

earity. In order to compare the macroscopic nonlinearities of three APC samples precisely, we doped the chromophore with an identical molar concentration into APC and poled them to measure the EO coefficient at 1300 nm.

Real time pole and probe method permits us to monitor EO signal. The effect of the geometry of the chromophore was investigated on EO properties. Dynamic and isothermal stabilities of the EO coefficients were investigated for comparing the NLO performance of the TCP chromophore.

Experimental

The synthetic procedure for three chromophores will be described in elsewhere.[23] All the chromophores were successfully synthesized and fully characterized. NMR spectroscopy and elemental analysis confirmed the structures of new chromophores.

Instrument. The absorption spectra of the chromophore solutions (solvent: chloroform, conc. 1×10^{-5} mole/L) were recorded with an UV-VIS spectrophotometer (HP 8453, photodiode array type λ = 190-1100 nm). Melting temperatures were measured using Perkin Elmer 7 DSC under nitrogen (rate of temperature: 5 °C). Thermal decomposition temperature was measured by Perkin Elmer 7 TGA under nitrogen (rate of temperature: 10 °C).

Spectroscopic ellipsometry measurement to determine the refractive indices at various wavelengths was performed on the thin film with incidence angles of 65, 70, and 75 degrees using a Woollam VASE model with autoretarder in the spectral range of 310-1550 nm (0.8-4.0 eV).

Electrochemical Analysis. The electrochemical experiments were carried out using on a EC-Epsilon (E2P) cyclic voltammetry. The voltammogram was obtained at 25 °C in anhydrous acetonitrile containing 0.1 M tetrabutylammonium hexafluorophosphate (Bu_4NPF_6) at the scan rate of 50 mV/s under an argon atmosphere. A working electrode was platinum (Pt). A counter electrode and a reference electrode were platinum wire and Ag/AgCl electrode, respectively. The ionization potential values were internally calibrated against the ferrocene/ferricinium couple for each experiment.

Material Processing for Electro-optic Study. The mixed solution (10 wt%) of chromophore and APC were prepared in cyclopentanone/cyclohexanone (1:1). The same number of chromophore (e.g. 4.56×10^{19} molecules in 0.1 g of APC) was doped in all APC samples. For studying EO effect, thin films (thickness: 2.2-2.5 μm) were fabricated on indium tin oxide (ITO) precoated glass with a filtered solution (0.2 μm Acrodisc syringe filter). For reflection measurement, we deposited a gold electrode on the surface of APC film (thickness: 100 nm) to fabricate sandwiched samples. The thickness of film was measured by using Surface Profilometer (KOSAKA, ET-3000).

Real Time Pole and Probe Measurement for Electro-optic Effect. We first measured the EO signal (I_m/I_c) of the samples by way of reflection technique after poling the sample following the conventional way.[24] An a.c. voltage (10 V_{rms} at 1 kHz) was applied to each sample to observe the modulated signal (I_m). The EO coefficient, "r_{33}" of the poled APC film was calculated by the following equation. The r_{33} value is directly proportional to I_m/I_c in eq. (1).

$$r_{33} = \frac{3\lambda I_m}{4\pi V_m I_c n^2} \frac{(n^2 - \sin^2\theta)^{1/2}}{\sin^2\theta} \sim I_m/I_c \quad (1)$$

where n is the refractive index at 1300 nm and I_m is the amplitude of EO modulation. V_m is the a.c. voltage applied to the sample and I_c is the intensity of the incident light where phase retardation is 90° between TE and TM mode.

For *in-situ* EO study, the sample was placed on the heater to apply the voltage combined of d.c. and a.c. components ($V(t) = V_{d.c.} + V_o \sin \omega t$). An a.c. voltage ($V_o \sin \omega t$) was added to the d.c. voltage ($V_{d.c.}$) for the simultaneous poling and probing of the EO signal (I_m/I_c). EO signal could be monitored during poling with increasing and decreasing sample temperature. The flowing current was measured using Keithley 2400 source meter as an ammeter.

Results and Discussion

Material Consideration. The structures of the TCP chromophores were illustrated in Figure 1. The chromophores forming a Donor-Acceptor (D-A) conjugated structure were obtained and the structure may result in the requisite ground-state charge symmetry. Incorporation of phenyl or thiophene lateral group to the molecular backbone and the use of a strong tricyano acceptor moiety could have affected microscopic NLO property. In order to prepare the DBAV-TCP, **1**, DBAVP-TCP, **2**, and DBAVT-TCP, **3**, we first synthesized dibutylphenylamine. A dibutyl group improves the solubility of the final chromophore in organic solvents and miscibility with APC, **4**.

Thermal analysis of each chromophore was performed

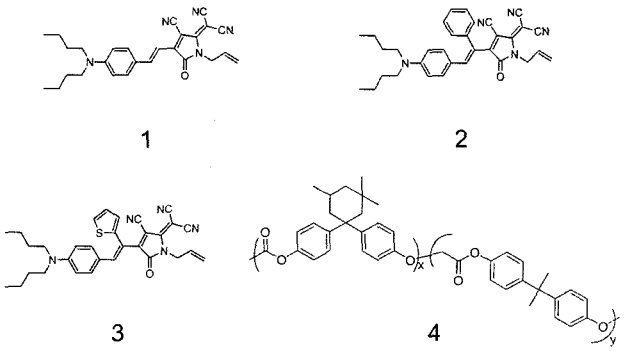

Figure 1. Structures of tricyanopyrrolidene-based nonlinear optical chromophores and host polymer, **1**, DBAV-TCP; **2**, DBAVP-TCP; **3**, DBAVT-TCP; **4**, amorphous polycarbonate.

Table I. Material Properties of the Chromophores Including the Theoretically Calculated Microscopic Parameters

	M.P. (°C)	T_d (°C)	λ_{max}(nm) ($CHCl_3$)	ε ($\times 10^4$)	μ ($\times 10^{-18}$ esu)	α(ave) ($\times 10^{-23}$ esu)	$\beta(0)$ ($\times 10^{-30}$ esu)	$\mu\beta(0)$ ($\times 10^{-48}$ esu)
DBAV-TCP	177	205	741	8.0	7.46	10.14	114.84	856.71
DBAVP-TCP	180	203	740	7.2	5.34	9.99	18.84	100.61
DBAVT-TCP	178	222	735	7.0	5.83	10.22	38.17	222.53

using a differential scanning calorimetry to obtain crystalline melting temperatures (T_m). Three chromophores have quite similar melting temperatures around 177-180 °C. Chromophore, **3** showed better thermal stability supported by a higher decompostion tempertaure (T_d) around 222 °C (see Table I).

UV-visible absorption spectroscopy revealed that DBAV-TCP had a λ_{max} of 741 nm in chloroform. Chromophores, **2** and **3** exhibit the absorption maximum (λ_{max}) at 740 and 735 nm in chloroform. However, chromophore, **1** shows relatively shorter cutoff wavelength around 820 nm, which implies the largest bandgap energy ($\Delta E_{spect.}$) (see Figure 2 and Table II). The absorption spectra of three NLO chromophores illustrate an important feature to have a very sharp low energy absorption edge relative to conventional chromophore such as (2-[3-cyano-4-(2-{5-[2-(4-dibutyl-amino-phenyl)-vinyl]-thiophenyl-2-yl}-vinyl)-5,5-dimethyl-5*H*-furan-2-yli-dene]-malononitrile (FTC).[25]

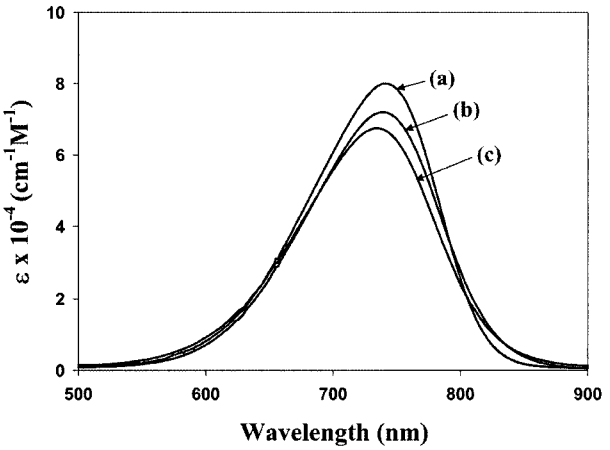

Figure 2. UV-Vis absorption spectra of the $CHCl_3$ solution samples. (a) DBAV-TCP, (b) DBAVP-TCP, and (c) DBAVT-TCP.

Electrochemical and Spectroscopic Analysis for the Molecular Energy Levels of Three Chromophores. We performed electrochemical analysis to determine the redox ionization potentials of the chromophores. Cyclic voltammetry was employed for estimating the energy levels of three TCP chromophores. The oxidation and reduction potentials are closely related to HOMO and LUMO energy levels and thus can provide important information regarding the magnitude of the energy bandgap.

They exhibit a single reversible or quasi-reversible oxidative wave in a positive energy mostly and an irreversible reductive peak in a negative energy. HOMO-LUMO gaps can be estimated from the oxidation and reduction potentials. However, the reduction peaks are not clear enough to assign the accurate ionization potential. We employed the optical bandgap calculated with the absorption edge of the electronic spectrum. We obtained the experimental HOMO, LUMO, and energy band gap in each chromophore after combining the results from two experiments. The electrochemical analysis results are illustrated in Table II including the data from spectroscopic measurement.

A small cathodic shift of both the oxidation and the reduction peak was observed in **2** and **3**. This can be explained by increase of the donor strength in principle. Although the conjugation of thiophene was not complete through the TCP acceptor unit, donability of the chromophore is likely to be enhanced.

Shortly, the molecular lateral group such as a thiophene and phenyl group effects the energy state of the final chromophores and decrease the bandgap energy to a small extent. The absorption spectroscopic and CV data are well consistent with an increase in electron delocalization with increasing donor strength.

Microscopic Nonlinearity and EO Properties of the APC Samples. In order to predict the microscopic nonlinear optical properties of the chromophores, we did molecular

Table II. Measured and Calculated Parameters from the Electrochemical and the Absorption Spectroscopic Experiments

	Electrochemical Analysis		Spectroscopic Analysis		
	E_{ox} (V vs. Fc/Fc^+)	E_{HOMO} (eV)	E_{LUMO} (eV)	$\Delta E_{Spect.}$ (eV)	$\lambda_{cut\text{-}off}$ (nm)
DBAV-TCP	-0.46	-5.26	-3.74	1.51	820
DBAVP-TCP	-0.43	-5.23	-3.73	1.49	827
DBAVT-TCP	-0.41	-5.21	-3.70	1.50	825

orbital calculation to determine quantum mechanical parameters. The geometry of the chromophore was first optimized by means of the MOPAC 2002 (CAChe version 5.04, PM3-Hamiltonian). The PM3 program was used for calculating the dipole moment, polarizability, and molecular hyperpolarizability in the ground state under the method of time-dependent Hartree-Fock (TDHF).

In Table I, the calculated dipole moments (μ), polarizabilities (α), and molecular hyperpolarizabilities (β) of three chromophores are well tabulated. The chromophores **2** and **3** showed incomparably smaller hyperpolarizability and $\mu\beta$ (0) than **1** in a gas state molecule. As is shown in optimized geometries of Figure 3, the large disruption of the planarity due to a lateral group is likely to induce the breakage of the conjugation through the molecular backbone. However, exact conformation of the chromophore in a solid state is still ambiguous to be defined.

We investigated the EO properties of the APC samples doped with three different chromophores. Before measuring the EO signal, we measured the refractive indices of the samples for calculating the accurate number of EO coefficient. Spectroscopic ellipsometry measurement was employed together with the absorption spectra of each film to determine the real and imaginary part of the refractive index at 1300 nm. Under identical measurement conditions, APC samples containing **1, 2,** and **3** showed refractive indices of 1.63, 1.64, and 1.64, respectively.

The EO coefficient, r_{33} was generally obtained by using the simple reflection technique.[20] All samples possess very little absorbance at the measured wavelength of 1300 nm. In order to observe an optimized EO signal, we performed real-time pole and probe method to examine the maximum EO effect. In this experiment, we applied the electric field (E_p = 70 V/μm) to the sample and no dielectric breakdown occurred during measurement. We applied the electric field $[E(t) = E_{d.c.} + E_o \sin \omega t]$ to the samples in order to measure the EO signal while heating the sample. The EO signal was recorded upto the maximum temperature at which the film was not broken down. The temperature was selected by repeated experiments using each sample. During EO signal measurement, we recorded a flowing current with the temperature, which is shown in Figure 4. In this report, the samples I, II, and III stand for the APC films bearing **1, 2,** and **3**, respectively.

The EO signal, (I_m/I_c), increases slowly as a temperature is raised. The temperature rate was set to be 5 °C/min. The maximum temperature is around 120 °C in the presence of 70 V/μm for comparing poling efficiency under an identical condition. In the cooling process, we observed relatively large decrement of EO signal in the sample I. However, the other two samples did not show that much decay. The resultant EO signal values of the sample II and III higher than that of the sample I under identical treatment conditions. This implies that the aligned chromophore, **1** can be relaxed due to larger electrostatic force over the poling force. Two samples II and III did not show that overwhelming effect over poling force so that the signal was almost sustained at a constant level. This is likely to be attributed to reduction of the electrostatic interaction by virtue of the molecular lateral group. Additionally, as we observed the energy levels of the chromophores, **2** and **3**, the donating property was slightly enhanced compared to **1**. Finally, the sample III exhibited highest r_{33} around 54 pm/V after poling at 100 V/μm although the microscopic nonlinearity ($\mu\beta$(0)) was relatively quite small.

The geometry of **1** was figured out to be quite planar as well as has much higher permanent dipole moment according to the theoretical calculation. We expect the strong competition between the electrostatic force and poling force by applying the electric field. Therefore, the poled chromo-

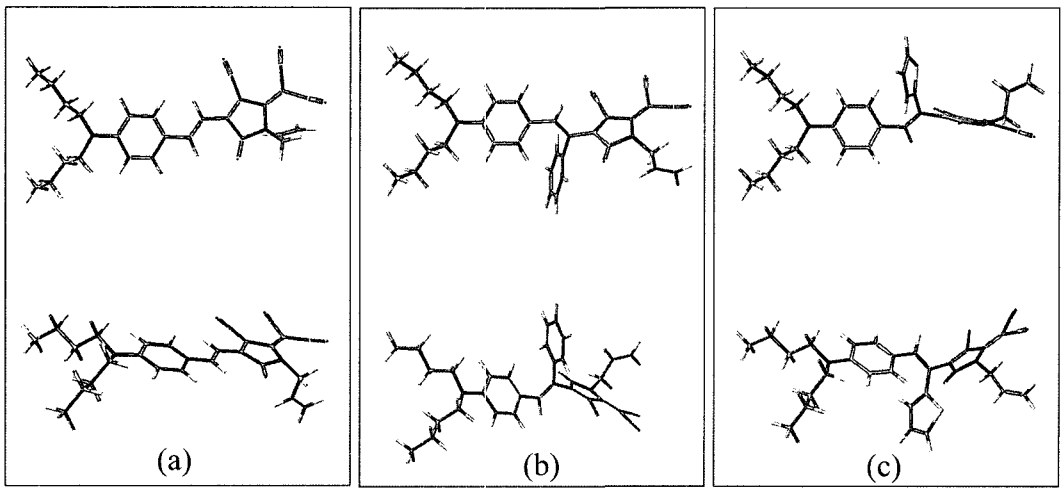

Figure 3. Geometries of the chromophores optimized in a gaseous state theoretically: (a) DBAV-TCP, (b) DBAVP-TCP, and (c) DBAVT-TCP.

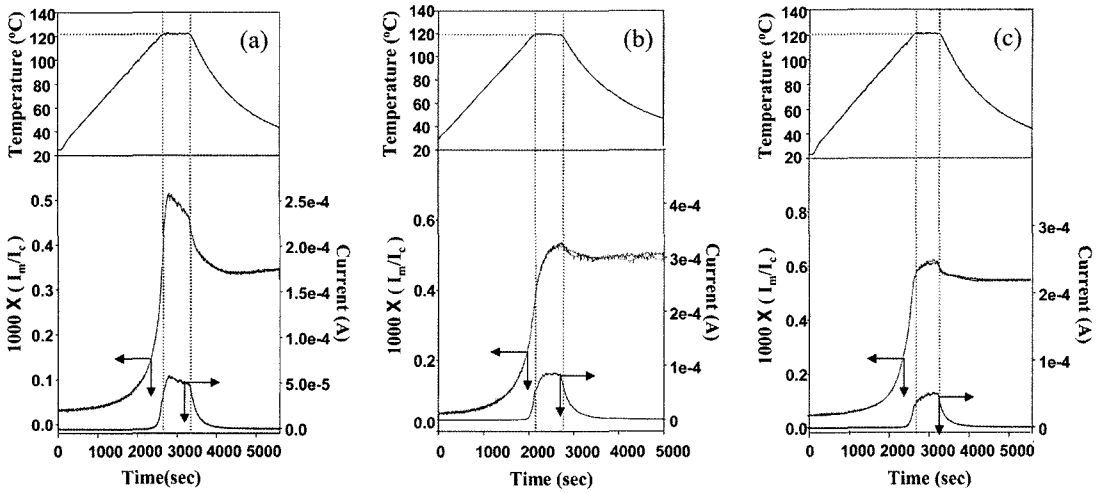

Figure 4. Temperature dependence of EO signal, I_m/I_c and flowing current during heating and cooling *chromophore: (a) DBAV-TCP, (b) DBAVP-TCP, and (c) DBAVT-TCP (E_p=70 V/μm).

phores exist in a highly strained conformation.

The sample II and III did show the increment under an isothermal condition and much smaller decrement of the signal during cooling stage (see Figure 4(b) and (c)). The chromophores **2** and **3** inherently seem to show the distorted molecular backbone structure interrupting a stable conjugation path, which is attributed to tethering the phenyl or thiophene unit in an ethylenic bond. Therefore, it reduces the molecular aggregation that increases the electrostatic interactive force between the chromophores. In the sample II and III, poling enforcement is dominant over the molecular interaction so that the signal can be sustained even during cooling process.

Resultantly, after cooling the sample, the EO coefficient, (r_{33}) was calculated again with the stabilized value of I_m/I_c. Although the microscopic nonlinearity of **1** is much higher theoretically and the same number of NLO active chromophore was doped in two samples, sample III with **3** showed relatively higher EO coefficient (~40-54 pm/V).

Relaxation Behavior of the EO Activity. We monitored the relaxation behavior of EO signal with sample temperature. The dynamic thermal stability of EO signal is shown in Figure 5. We observed the transition temperature in each decaying curve. The samples II and III showed higher transition temperature which implies a better stability of EO effect than the sample I. It is well consistent with the transition temperature in the dynamic rising behavior of EO signal.

In order to compare the isothermal stability of three samples precisely, we traced the decaying behaviors of EO signal without poling field at 100 °C. In order to investigate the decaying behavior of (I_m/I_c) and to prevent from the relaxation of molecular alignment during heating and cooling, we applied a dc electric field and raised the temperature to 120 °C. After storing the sample for 10 min for thermal equilibrium, we decreased the temperature to 100 °C and stored the sample for another 10 min. Then, the poling field

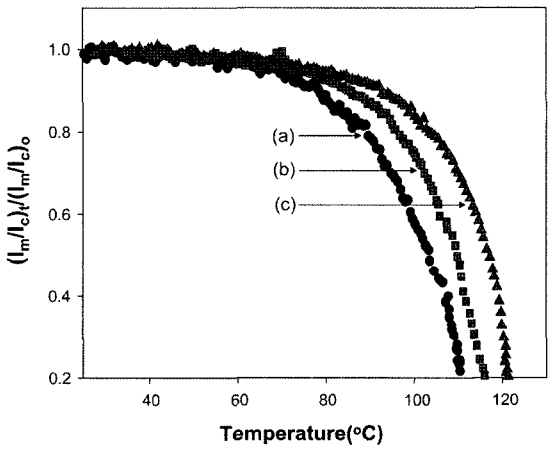

Figure 5. Dynamic relaxation behavior of EO signal, I_m/I_c during heating *chromophore: (a) DBAV-TCP, (b) DBAVP-TCP, and (c) DBAVT-TCP.

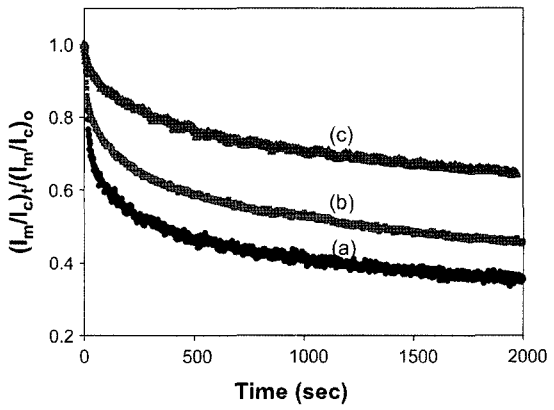

Figure 6. Isothermal relaxation behavior of the E/O signal at 100 °C. *chromophore: (a) DBAV-TCP, (b) DBAVP-TCP, and (c) DBAVT-TCP.

Table III. Calculated Parameters of the Isothermal Relaxation Curves at 100 °C and the Determined EO Coefficients

	Calculated Parameters for EO Relaxation			r_{33} (pm/V)	
	τ (=1/k, sec)	β	$<\tau>$ (sec)	70V/μm[a]	100 V/μm[a]
DBAV-TCP	189.75	0.3886	684.33	19	-
DBAVP-TCP	826.45	0.5307	1489.509	32	-
DBAVT-TCP	1111.11	0.3528	5436.187	40	54

[a]Poling field.

was switched off and an ac voltage was applied to record EO signal. The decaying data of each sample are plotted in Figure 6. The decaying curves were analyzed using Kohlrausch-Williams-Watts (KWW) stretched exponential function (eq. (2)).

$$[(I_m/I_c)_t/(I_m/I_c)_o] = \exp(-(t/\tau)^{\beta}) + [(I_m/I_c)_\infty/(I_m/I_c)_o] \quad (2)$$

where $(I_m/I_c)_o$ is the maximum EO signal at $t = 0$ sec and $(I_m/I_c)_\infty$ is the lowest signal at time = ∞ sec.

Using the above equation, we could determine a relaxation time, τ and a stretching parameter, β. Using those two parameters, we finally calculated an average time constant, $<\tau> = (\tau/\beta)\,\Gamma\,(1/\beta)$. The determined parameters are shown in Table III.

Shortly, the poled molecular order in sample I was randomized much faster. This can be explained as follows. In sample I, almost perfectly planar chromophore, **1** is easier to be self-associated in an antiparallel manner so that the phase separation can occur after poling at a high temperature, which is likely to show entropy driven lower critical solution temperature (LCST) behavior in polymer blends. On the while, **3** shows good miscibility to be phase separated scarcely at a poling temperature due to unique geometrical conformation. The critical temperature for phase separation may be relatively higher than that of **1**.

Another conjecture is that the oriented dipolar **1** molecules were trapped in a strained conformation during poling. Thus, it can return more easily to the isotropic state partly due to the electrostatic interaction as well as free volume shrinking effect. The existence of residual strain from an equilibrium state during poling enforced the oriented dipoles for more rapid relaxation than the cases in the samples II or III. However, it is hard to be proved by any spectroscopic study or thermal analysis. We make much attempt to monitor the relaxation behavior of EO signal both at the temperatures below and above T_g of EO matrix for understanding this phenomenon.

Conclusions

We employed the tricyanopyrrolidene-based chromophore to investigate the effect of the chromophore type within the host polymer on EO effect. Unlike static poling and EO measurements, the real time pole and probe method both allowed us to measure the maximum EO coefficient and provided much helpful information to characterize the materials property. The DBAVT-TCP containing APC sample showed relatively higher EO property and relatively high thermal stability. That can be understood by the fact that the distorted molecules lessened the electrostatic force not comparable to poling force and good miscibility with APC polymer structure. We expect far higher EO coefficient as well as good thermal stability under poling at a higher field than that we used in this study.

Acknowledgements. This work was supported by the Ministry of Commerce, Industry, and Energy (Contract# 10022811-2005-12). Prof. D. H. Choi thanks the Seoul R&BD Program (2005-2006) for financial support.

References

(1) L. R. Dalton, A. W. Harper, R. Ghosn, W. H. Steier, M. Ziari, H. Fetterman, Y. Shi, R. V. Mustacich, A. K-Y. Jen, and K. J. Shea, *Chem. Mater.*, **7**, 1060 (1995).
(2) L. R. Dalton, A. W. Harper, B. Wu, R. Ghosen, J. Laquindanum, Z. Liang, A. Hubbel, and C. Xu, *Adv. Mater.*, **7**, 519 (1995).
(3) L. R. Dalton, A. Harper, A. Ren, F. Wang, G. Todorova, J. Chen, C. Zhang, and M. Lee, *Ind. Eng. Chem. Res.*, **38**, 8 (1999).
(4) C. Samyn, T. Verbiest, and A. Persoons, *Macromol. Rapid Commun.*, **21**, 1 (2000).
(5) K. R. Yoon, H. S. Lee, B. K. Rhee, and C. S. Jung, *Macromol. Res.*, **12**, 581 (2004).
(6) P. G. Lacroix, *Chem. Mater.*, **13**, 3495 (2001).
(7) K. V. Katti, K. Raghuraman, N. Pillarsetty, S. R. Karra, R. J. Gulotty, M. A. Chartier, and C. A. Langhoff, *Chem. Mater.*, **14**, 2436 (2002).
(8) P. Zhu, M. E. van der Boom, H. Kang, G. Evmenenko, P. Dutta, and T. J. Marks, *Chem. Mater.*, **14**, 4982 (2002).
(9) A. Facchetti, A. Abbotto, L. Beverina, M. E. van der Boom, P. Dutta, E. G. Vmenenko, G. A. Pagani, and T. J. Marks, *Chem. Mater.*, **15**, 1064 (2003).
(10) F. Chaumel, H. Jiang, and A. Kakkar, *Chem. Mater.*, **13**, 3389 (2001).
(11) M. Ahlheim, M. Barzoukas, P. V. Besworth, M. Blanchard-Desce, A. Fort, Z.-Y. Hu, S. R. Marder, J. W. Perry, C. Runser, M. Staehelin, and B. Zysset, *Science*, **271**, 335 (1996).

(12) S. R. Marder, L.-P. Cheng, B. G. Tiemann, A. C. Friedli, M. Blanchard-Desce, J. W. Perry, and S. J. KindhØj, *Science*, **263**, 511 (1994).
(13) M. Trollsas, C. Orrenius, F. Sahlen, U. W. Gedde, T. Norin, A. Hult, D. Hermann, P. Rudquist, L. Komitov, S. T. Lagerwall, and J. Lindstrom, *J. Am. Chem. Soc.*, **118**, 8542 (1996).
(14) S. Song, S. J. Lee, B. R. Cho, D.-H. Shin, K. H. Park, C. J. Lee, and N. Kim, *Chem. Mater.*, **11**, 1406 (1999).
(15) E. M. Breitung, C.-F. Shu, and R. J. McMahon, *J. Am. Chem. Soc.*, **122**, 1154 (2000).
(16) P. R. Varanasi, A. K.-Y. Jen, J. Chandrasekhar, I. N. N. Namboothiri, and A. Rathna, *J. Am. Chem. Soc.*, **118**, 12443 (1996).
(17) I. D. L. Albert, T. J. Marks, and M. A. Ratner, *J. Am. Chem. Soc.*, **119**, 6575 (1997).
(18) M. Q. He, T. M. Leslie, and J. A. Sinicropi, *Chem. Mater.*, **14**, 2393 (2002)
(19) A. Grunnet-Jepsen, C. L.Thompson, and W. E.Moerner, *Science*, **277**, 549 (1997).
(20) S. R. Marder, B. Kippelen, A. K.-Y. Jen, and N. Peyghambarian, *Nature*, **388**, 845 (1997).
(21) B. W. You, Z. Hou, and L. Yu, *Adv. Mater.*, **16**, 356, (2004).
(22) S.-H. Jang, J. Luo, N. M. Tucker, A. Leclercq, E. Zojer, M. A. Haller, T.-D. Kim, J.-W. Kang, K. Firestone, D. Bale, D. Lao, J. B. Benedict, D. Cohen, W. Kaminsky, B. Kahr, J.-L. Bredas, P. Reid, L. R. Dalton, and A. K.-Y. Jen, *Chem. Mater.*, **18**, 2982 (2006)
(23) M. J. Cho, S. K. Lee, J. H. Lim, C. S. Hong, and D. H. Choi, *J. Mater. Chem.*, submitted (2006).
(24) C. C. Teng and H. T. Man, *Appl. Phys. Lett.*, **56**, 1734 (1990).
(25) C. Zhang, C. Wang, L. R. Dalton, H. Zhang, and W. H. Steier, *Macromolecules*, **34**, 253 (2001).